Undergraduate Final Project

Fitting Gaussian Curves on Particle Images for Density Estimation

Lucas Mendes Massa

advised by
Prof. Dr. Tiago Figueiredo Vieira
Prof. Dr. Ícaro Bezerra Queiroz de Araújo

UNIVERSIDADE FEDERAL DE ALAGOAS
Institute of Computing

FITTING GAUSSIAN CURVES ON PARTICLE IMAGES FOR DENSITY ESTIMATION

Undergraduate Final Project submited to the Institute of Computing at the Universidade Federal de Alagoas as a partial requirement for obtaining the degree of Computer Engineer.

Lucas Mendes Massa

Advisor: Prof. Dr. Tiago Figueiredo Vieira
Co-advisor: Prof. Dr. Ícaro Bezerra Queiroz de Araújo

Examining Board:

Ícaro Bezerra Queiroz de Araújo   Prof. Dr., UFAL
Allan de Medeiros Martins   Prof. Dr., DEE-UFRN

Maceió, Alagoas
March 6th, 2023

Trabalho de Conclusão de Curso – TCC

Formulário de Avaliação

Curso: _____

Nome do Aluno

L	U	C	A	S		M	E	N	D	E	S		M	A	S	S	A		

Nº de Matrícula

					1	8	1	1	2	2	1	1

Título do TCC (Tema)

Fitting Gaussian Curves on Particle Images for Density Estimation

Banca Examinadora

Tiago Figueiredo Vieira
Nome do Orientador

Ícaro Bezerra Queiroz Araújo
Nome do Professor

Allan de Medeiros Martins
Nome do Professor

Documento assinado digitalmente
gov.br TIAGO FIGUEIREDO VIEIRA
Data: 20/03/2023 10:34:01-0300
Verifique em https://validar.iti.gov.br

Documento assinado digitalmente
gov.br ICARO BEZERRA QUEIROZ DE ARAUJO
Data: 20/03/2023 11:19:04-0300
Verifique em https://validar.iti.gov.br

Documento assinado digitalmente
gov.br ALLAN DE MEDEIROS MARTINS
Data: 20/03/2023 11:40:22-0300
Verifique em https://validar.iti.gov.br

Data da Defesa	Nota Obtida
17/ Março/ 2023	10,00 (Dez)

Observações
_____
_____
_____
_____

Coordenador do Curso
De Acordo

Documento assinado digitalmente
gov.br LEANDRO DIAS DA SILVA
Data: 21/03/2023 16:17:11-0300
Verifique em https://validar.iti.gov.br

Assinatura

Acknowledgements

Words cannot express my gratitude to my family, especially my parents, José and Maria Jaqueline, and my grandparents, Hércules and Nadja. They have always given me all the support I needed to achieve my goals in addition to teaching me, from an early age, that studying should always be taken seriously.

I would like to express my deepest appreciation to my advisor, Prof. Tiago Vieira, for trusting in me and for always being present during the development of this work. I extend my sincere thanks to all the professors who contributed to my academical formation, in particular Prof. Ícaro Bezerra, who advised me a lot in the final phase of graduation and was always available to help in any possible way. I'm also grateful to the examining board, specially Prof. Allan Martins.

Finally, I could not have undertaken this journey without the support from my girlfriend, Luana, who always helped me in my moments of difficulty, encouraging me to keep going during these many years of university. Special thanks also to my classmates, with whom I developed a great partnership throughout the course. I will have them as friends for the rest of my life.

March 6th, 2023, Maceió - AL

Resumo

No presente trabalho utilizou-se um dispositivo impresso em 3D para medir a densidade de uma micropartícula fazendo uso de acustofluídica, a qual consiste em aplicar ondas sonoras para prender partículas no espaço livre. Inicialmente, a partícula fica presa no plano focal do microscópio (sem desfoque). Em seguida, os transdutores são desligados e a partícula ao longo do fluido, aumentando seu diâmetro devido ao desfoque causado pela distância até a lente. Esse aumento de diâmetro ao longo do tempo fornece sua velocidade, que pode, por sua vez, ser usada para calcular sua densidade. Anotar manualmente o diâmetro nas imagens capturadas é uma tarefa tediosa e sujeita a erros. Isso acontece devido ao alto ruído presente nas imagens, principalmente nos últimos quadros onde o desfoque é alto. Dessa forma, usamos um processo de ajuste de modelo Gaussiano 2D para estimar o diâmetro da partícula em diferentes quadros de profundidade. Para encontrar os diâmetros, inicialmente realizamos o ajuste dos parâmetros Gaussianos com Algoritmo Genético em cada quadro da trajetória da partícula registrada para evitar mínimos locais. Em seguida, refinamos o ajuste com Gradient Descendente usando Tensorflow para compensar qualquer aleatoriedade presente no ajuste do Algoritmo Genético. Validamos o método recuperando a densidade de uma partícula conhecida com desempenho satisfatório.

Palavras-chave: **Estimação de Densidade de Partículas, Algoritmo Genético, Gradiente Descendente, Ajuste de Gaussiana 2D, Acustofluídica.**

Abstract

We use a 3D printed device to measure the density of a micro-particle with acoustofluidics, which consists in using sound waves to trap particles in free space. Initially, the particle is trapped in the microscope's focal plane (no blur). Then the transducers are shut off and the particle falls inside the fluid, increasing its diameter due to defocus caused by the distance to the lens. This increase in diameter along time provides its velocity, which can, in turn, be used to compute its density. To manually annotate the diameter in the recorded images is a tedious task and is prone to errors. That happens due to the high noise present in the images, specially in the last frames where the defocus is high. Because of that, we use a 2D Gaussian model fitting process to estimate the particle diameter throughout different depth frames. To find the diameters, we initially perform the Gaussian parameters fit with Genetic Algorithm in each frame of the recorded particle trajectory to avoid local minima. Then we refine the fit with Gradient Descent using Tensorflow in order to compensate for any randomness present in the fit of the Genetic Algorithm. We validate the method by retrieving a known particle's density with acceptable performance.

Keywords*: *Particle Density Estimation, Genetic Algorithm, Gradient Descent, 2D Gaussian Fitting, Acoustofluidics.

List of Figures

List of Symbols

$\overrightarrow{F}_{gravitational}$ Gravitational force.

$\overrightarrow{F}_{viscosity}$ Viscosity force.

$\overrightarrow{F}_{buoyancy}$ Buoyancy force.

g Gravitational acceleration.

π Pi mathematical constant.

r Spherical particle radius.

$\rho_{particle}$ Denstity of the particle.

ρ_{fluid} Density of the fluidic medium.

μ Dynamic viscosity of the fluidic medium.

v Particle velocity during fall.

$\hat{k}$ Unitary vector in z-axis.

p Gaussian amplitude.

μ_x Position of the Gaussian's center in the image along the (horizontal) x-axis.

μ_y Position of the Gaussian's center in the image along the (vertical) y-axis.

σ Standard deviation of the Gaussian.

σ^2 Variance of the Gaussian.

$f(X)$ Multivariable function.

$\nabla f(X)$ Gradient of a function.

$\frac{\partial f}{\partial x_n}(X)$ Partial derivative relative to the nth function variable.

α Learning rate.

Y_i ith expected output.

$\hat{Y}_i$ ith obtained ouput.

z Gaussian function.

I Particle image.

L Loss function.

W Image width.

H Image height.

A_i Area for the particle in the ith image of a sequence.

$A_{relative}$ Relative area of a particle in a image.

List of Abbreviations

SNR   Signal-to-Noise Ratio

RGA   rotating gliding arc

SPECT   Single-Photon Emission Computerized Tomography

GA   Genetic Algorithm

GD   Gradient Descent

MSE   Mean Squared Error

Summary

Chapter 1

Introduction

1.1   Motivation

Studying the density of nanometer scale particles is of great importance in many science fields. It can be noted that, in biology and medicine, the analysis of a cell density may lead to a series of informations about the cell. As stated by Bryan et al. (2010), cell volume is coupled to mass and energy requirements that control cell division and survival. In this way, by accurately measuring the size of a cell one can understand cycle position of a cell and also identify its type. As the cell volume is directly related to mass and density, changes in its size can be measured as variations in the density. In line with what was reported above, Zhao et al. (2014) argues that density measurements can provide an effective evaluation mechanism to monitor cell responses to external stimuli such as drugs and environmental changes.

Therefore, scientists began to investigate effective ways of measuring the density of isolated particles. In this way, the separation of particles of interest from complex mixtures to play a crucial role, as shown by Fan et al. (2022) and Li et al. (2015). Recently, acoustofluidic, which consists in using sound waves propagating through some fluid medium, has been used in areas like clinical diagnostics Wang et al. (2021) and therapeutics Bose et al. (2015) due to its capability of trapping particles having specific physical characteristics. By observing isolated particles or conglomerates (colloids), one can confirm the occurrence of specific reactions and determine whether a given pathogen is present in a body fluid sample using a microscope, for instance.

Traditionally, several techniques have been used to separate particles, such as those based on centrifuges, which is time-consuming, can cause substantial material loss and alter cell functions Fan et al. (2022). In contrast, with a carefully designed acoustic field, one can separate target cells embedded in a complex liquid, which has been validated as a viable, contact-less, bio-compatible and label-free technology. Additionally, by incorporating automation and tackling limitations of conventional strategies, isolating sub-micron

1

bio-particles can potentially accelerate the development of Point-of-Care devices.

In this work, we use an acoustofluidic 3D printed device (fluid chamber) to measure the density of polystyrene beads. The device is initially filled with a fluid in which the analytes are embedded. Transducers are then excited to generate an acoustic field responsible for "trapping" the particle in a given position. A microscope is used to acquire images of the cells as exemplified in Fig. 1.1, where the "trapped" particle is represented by the first image (top-left). After the acoustic field is disabled, the particle falls along time, causing a strong blur as shown in the middle and final columns in Fig. 1.1, since the particle is no longer within the microscope focus plane. By observing the fall velocity (depth per moment in time) and using a calibration curve obtained in beforehand that relates the particle's diameter to depth, one can compute a good estimate of the cell's density (*cf.*, Chapter 3).

Figure 1.1: Captured images of a falling particle. The blur gradually increases along the process. First row: original images captured by a microscope. Middle row: Same images with enhanced contrast. Last row: particles fitted by a curve.
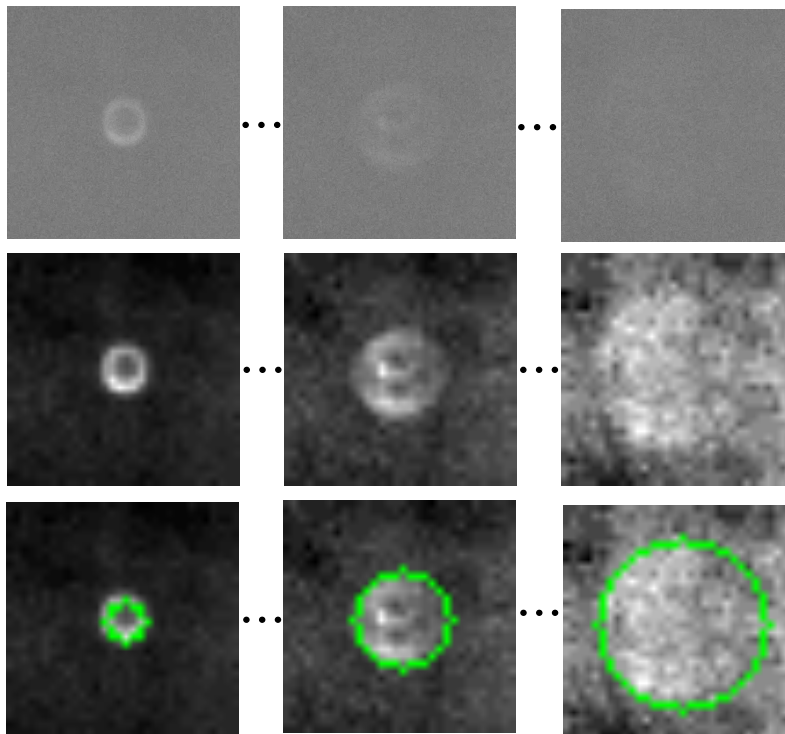
Source: The authors

Unfortunately, annotating cell's diameters on different images is a manual process due to a very low Signal-to-Noise Ratio (SNR) inherent to the blurring process caused by the particle fall and short Depth-of-Field of the microscope optical apparatus. Therefore, one must manually annotate each image in both stages of calibration and dynamic measurement. Manually annotating images is a time-consuming and cumbersome process due to many characteristics. It is prone to human error and fatigue, rendering automation and development of Point-of-Care devices unfeasible.

The bead's diameter is related to the depth, which can provide information regarding the velocity of the fall (depth per time). It can be shown that the velocity with which the particle falls into the medium, along with other quantities can provide the particle's density value (*cf.* Chapter 2). Therefore, we propose a method capable of measuring the particle's diameters during its fall. Due to the amount of noise, we found that fitting a 2D Gaussian in a Gradient Descent fashion can provide reasonable performance in the final densisty measurement.

Fitting a Gaussian onto a signal (image) is a method that can be applied on different scenarios for different purposes. For instance, Ananthanarasimhan et al. (2022), used the technique to estimate the diameter of discharges viewed by High Speed Cameras (HSC) to characterize a rotating gliding arc (RGA) reactor. Kizel et al. (2015) proposed a method for fully constrained spatially adaptive spectral unmixing for the localization of endmembers. Lei et al. (2016) used a 2D Gaussian fitting procedure to locate motion-blurred, weak celestial objects in images for the purpose of orbital debris monitoring. Dai et al. (2010) used the method to estimate the Point Spread Functions of different optical apparatus and ultimately increase the resolution of Single-Photon Emission Computerized Tomography (SPECT) to sub-millimeter range. Anniballe and Bonafoni (2015) proposed a Gaussian fitting procedure aimed at analyzing remotely sensed thermal multi-resolution images to monitor variations in urban occupancy throughout area and time. Bui et al. (2015) proposed the segmentation of murine tumor from noisy ultrasound clinical images using Gaussian distribution to model local intensities.

In this context, a Computer Vision strategy capable of automatically measuring cell diameter on noisy images was studied. This simple, yet effective, method is based on 2D Gaussian fitting using Genetic Algorithm (GA) and a subsequent refinement with Gradient Descent (GD) method. Experiments showed that the methodology provides a satisfactory performance and can eventually contribute to the development of fully automated devices.

1.2   Objectives

1.2.1   General Objectives

Evaluate the performance of a 2D Gaussian curve fitting approach on the task of particle density measurement based on microscope images captured from an acoustofluidic micro-cavity.

1.2.2   Specific Objectives

1. Calculate a calibration curve that relates particle height and particle area;

2. Implement a 2D Gaussian curve fitting algorithm that receives as input a preprocessed microscope image;

3. Optimize Gaussian curve hyperparameters through Genetic Algorithm and Gradient Descent approaches;

4. Use the calculated curves to estimate the particle area and generate a height curve based on the calibration;

5. Derivate the particle velocity from the height curve and use it to estimate the particle density.

1.3   Work Organization

This work was organized into chapters that report the steps followed during the development of the solution, going into theoretical details and application of the technologies involved. Chapter 2 presents a theoretical basis on the involved physical concepts, the curve fitting approach, the used hyperparameter optimization strategies and on the applied evaluation metrics. Chapter 3 describes how all the steps in this work were developed, more specifically, the acquisition of the database, the generation of a calibration curve, the data preprocessing, the construction of curve fitting models and their opimization based on two different algorithms. Chapter 4 is dedicated to exposing and discussing the obtained results. Finally, conclusions about the work are presented.

Chapter 2

Theoretical Foundation

2.1 Physical Background

The density of a particle embedded in a liquid affects the rate in which it falls (in distance per time). The relation between fall rate and density can be found by analyzing the problem's dynamics, which, for a particle embedded in a fluidic medium, is ruled by a specific set of forces. As explained by Zhao et al. (2014), forces caused by particle-to-particle interaction, thermal effects and Brownian motion can be disregarded due to their low order of magnitude when compared with other forces that act on the system. Thus, the resulting force that pulls the particle down along the vertical axis can be expressed as a combination of gravitational, viscosity and buoyancy forces:

$$\sum \overrightarrow{F} = \overrightarrow{F}_{gravitational} + \overrightarrow{F}_{viscosity} + \overrightarrow{F}_{buoyancy} \tag{2.1}$$

Considering that the vertical axis is pointed downward and approximating the particle as a perfect sphere, one can express the forces mentioned above as

$$\overrightarrow{F}_{gravitational} = \left(\frac{4}{3}\pi g r^3 \rho_{particle} \right) \hat{k} \tag{2.2}$$

$$\overrightarrow{F}_{buoyancy} = \left(-\frac{4}{3}\pi g r^3 \rho_{fluid} \right) \hat{k} \tag{2.3}$$

$$\overrightarrow{F}_{viscosity} = (6\pi r \mu v)\hat{k}, \tag{2.4}$$

where $\rho_{particle}$ is the particle's density, ρ_{fluid} is the fluidic medium's density, r is the sphere's radius, μ is the fluid's dynamic viscosity and v is the particle's velocity during fall.

Therefore, by applying Newton's second law, considering v as particle's velocity along z axis and solving the resulting differential equation for the intensities of the forces defined

above, the following expression is found:

$$v(t) = \frac{2r^2 g(\rho_{particle} - \rho_{fluid})}{9\mu}(1 - e^{-\frac{t}{\tau}}) \tag{2.5}$$

Since $\tau = m/6\pi r \eta K$ is very small, the exponential term from Equation (2.5) can be ignored. Manipulating the resulting expression, one can find the final relation between particle density and fall velocity:

$$\rho_{particle} = \frac{9\mu v}{2r^2 g} + \rho_{fluid}. \tag{2.6}$$

I.e., one can compute the particle's density (in kilograms per cubic meters) if its fall velocity and its radius are known. During the course of this work 10μm diameter polystyrene beads were used, which have a well known density of around 1050 kg·m^{-3}.

2.2 Gaussian Function

Figure 2.1: Plot of a 2D Gaussian function
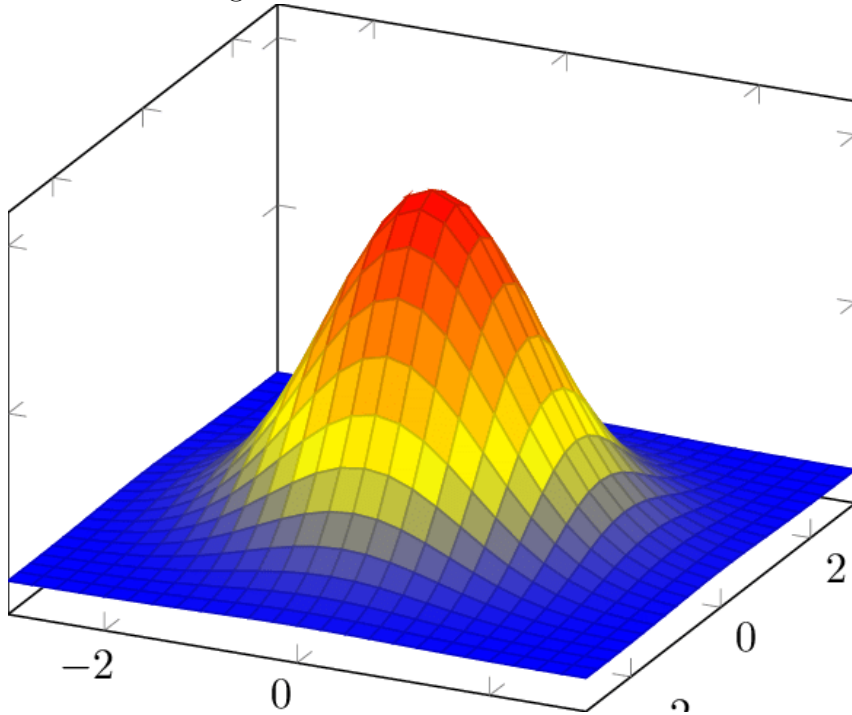
Source: Byttner (2019).

The Gaussian function is a very common approximation for the probability distribution of many observable phenomenons. This function results in a "bell shaped" curve and is defined by the following equation:

$$y(x) = \frac{1}{\sigma\sqrt{2\pi}}e^{-\frac{(x-\mu)^2}{2\sigma^2}} \tag{2.7}$$

Considering a multivariable distribution, this function can be extended to have x and y as inputs, delivering a curve $z(x, y)$ whose format can be seen in Fig 2.1. The particles investigated during this work tend acquire a circular shape once the image contrast is enhanced, providing the possibility to approximate their shape with a 2D Gaussian curve. This happens due to the fact that the Gaussian value in a specific (x, y) coordinate can be seen as the intensity of a grayscale image pixel with the same coordinates.

Thus, in the conducted experiments, we generate images by applying the following 2D Gaussian function expression:

$$z(x, y) = p \, \exp\left[- \left(\frac{(x - \mu_x)^2}{2\sigma^2} + \frac{(y - \mu_y)^2}{2\sigma^2} \right)^4 \right] \tag{2.8}$$

where:

- p: Gaussian amplitude.

- μ_x: Position of the Gaussian's center in the image along the (horizontal) x-axis.

- μ_y: Position of the Gaussian's center in the image along the (vertical) y-axis.

- σ: Standard deviation of the Gaussian (proportional to the radius of the image)

2.3 Hyperparameter Optimization

As stated above, this work studies a Gaussian function fitting approach. From Eq. (2.8), we can consider p, μ_x, μ_y and σ^2 as curve parameters. This turns finding the Gaussian that best fits an specific particle image into a complicated task due to the high range of values that this parameters can assume. A common approach for solving such class of problems is using optimization algorithms and will thus be used during the course of this work, more specifically Genetic Algorithm and Gradient Descent approaches.

2.3.1 Genetic Algorithm

Genetic Algorithms (GA) are a common choice for performing optimization tasks. This kind of algorithms are inspired by evolutionist theory, where natural selection keeps alive only the individuals that are more adapted to the environment and give them the opportunity to pass their genes to future generations. As exposed by Konak et al. (2006), in the GA formalism each individual is represented by a vector called *chromosome*. Chromosomes vectors are formed by values called *genes*. Each chromosome is considered to be a solution to the problem which is being optimized and are grouped in a set called *population*. The chromosome vectors generally are randomly initialized and through the combination of their genes, in a iterative process, converge to an optimized solution.

During this iterative process, two main operations are conduced: *crossover* and *mutation*. Firstly, in the crossover operation, two chromosomes combine their genes to generate a new one. Lastly the mutation introduces the chance of random changes to the genes, which also happen in nature. At each iteration only the most adapted individuals are used to perform the crossover operation. This metric of how much an individual is adapted to the problem is called *fitness* and is calculated through a function that is defined according to the optimization problem necessities.

2.3.2 Gradient Descent

Differential calculus defines the gradient of a function as a vector that indicates the direction to move from the current input parameters point so that one can get the greatest increase rate. Considering a multivariable function $f(X)$, where $X = [x_1, x_2, ..., x_{n-1}, x_n]$, this vector can be calculated by applying the following equation:

$$\nabla f(X) = (\frac{\partial f}{\partial x_1}(X), \frac{\partial f}{\partial x_2}(X), ..., \frac{\partial f}{\partial x_{n-1}}(X), \frac{\partial f}{\partial x_n}(X)) \tag{2.9}$$

Thus, in a optimization loop, one can minimize the function value by updating the parameters to a direction opposite to the gradient of current input vector. This approach is called *Gradient Descent* and is widely used in the *Machine Learning* field to find the best solution for a problem by minimizing a *loss function* that fits the scenario. Considering that we have a particle image I and we want to approximate it by a Gaussian curve $z(\mu_x, \mu_y, p, \sigma^2)$, our goal is to find μ_x, μ_y, p and σ^2 values that minimize a chosen loss function, which evaluates how far the generated curve is from the desired one.

Therefore, assuming $w = [\mu_x, \mu_y, p, \sigma^2]$ as an input vector, we can minimize the loss by updating it's values in a iterative process by using the following expression

$$w_{i+1} = w_i - \alpha \nabla_w L(I, z(w)) \tag{2.10}$$

where α is called learning rate and is responsible for determining the update step size at each iteration. $L(I, z(w))$ is the loss function, which receives as input the generated Gaussian $z(w)$ and the target image I. Finally $\nabla_w L$ represents the gradient of the loss function relative to the input vector w.

2.4 Evaluative Metrics

The task of fitting a 2D Gaussian curve consists of finding each pixel value in order to generate the Gaussian that comes closest to the particle image. Thus, it can be classified as a regression problem, leading to the usage of regression related functions during the performance evaluation.

2.4.1   Mean Squared Error (MSE)

The Mean Squared Error is a very common evaluation metric for regression models. This metric is used during the optimization steps as a loss function. It consists of the mean of the squared difference between expected and obtained outputs.

$$MSE = \frac{1}{N} \sum_{i=i}^{n} [Y_i - \hat{Y_i}]^2 \tag{2.11}$$

However, as we are dealing with a image regression, the concept above needs to be extended to two input variables. Thus, the MSE ends up being the mean of the squared difference between each pixel from expected and obtained images. Therefore, considering $z(x, y)$ and $I(x, y)$ as the pixel value for a given (x, y) coordinate for the generated Gaussian and the target image, respectively, the MSE formula can be defined as follows:

$$MSE = \frac{1}{WH} \sum_{x=1}^{W} \sum_{y=1}^{H} [I(x, y) - z(x, y)]^2 \tag{2.12}$$

where W and H are, respectively, images' width and height values.

Chapter 3

Methodology

3.1 Image Acquisition

The experiments were done by using images acquired from a microscope attached to a 3D printed device that contains a acoustofluidic chamber. This device is capable of levitating the particle while acquiring images through the microscope. When the levitation is interrupted the particle fall along the fluidic medium, causing the particle to gradually defocus in the consecutive images.

3.1.1 Hardware

For the acoustofluidic device, a cylindrical structure was fabricated using a 3D printer (*cf.*, Fig. 3.1a) Santos et al. (2021). A small disk with a diameter of 4mm and a height of 750μm was cast inside the cylindrical structure and top sealed by a glass cover which also acted as an acoustic reflector (*cf.*, Fig. 3.1b). This disk was used as an resonant chamber inside which particles were placed. A small inlet hole could be used to fill the chamber with fluid solutions of particles. This solutions could later be removed by an outlet hole. To deliver our experiments we used a fluidic solution with density and dynamic viscosity values of 997 kg·m^{-3} and 0.89×10^{-3} Pa·s, respectively. At the bottom of the acoustic chamber a circular piezoelectric actuator, with a diameter of 25mm, was attached. When the actuator is turned on, an acoustic standing wave is produced inside the resonant chamber (*cf.*, Fig. 3.1c). This creates an acoustic radiation force that traps the particles in a standing wave node, which has a height of approximately 95×10^{-6}m from chamber's bottom. An optical microscope is placed above the cylindrical structure such that confocal plane matches the wave node where particles are levitated. Turning off the actuator causes the acoustic forces to be extinguished (*cf.*, Fig. 3.1d), so the particles fall within the fluidic medium. As the particles fall, they gradually move away from microscope's confocal plane, becoming increasingly blurry in acquired images.

Figure 3.1: (a) Diagram of the used hardware. (b) Cross-section cut illustration of the device shown in (a). (c) When the actuator is on, a standing wave is generated and the particle is trapped in the microscope confocal plane. (d) When the actuator is turned off, the wave vanishes and the particle falls downwards presenting what we call a *dynamic* behaviour.
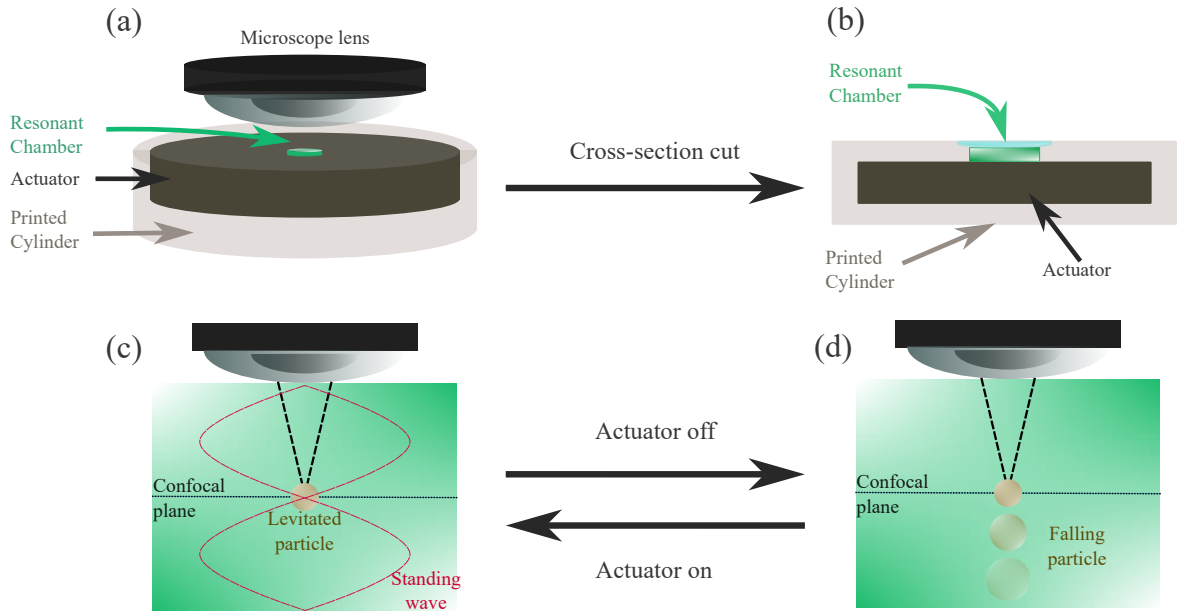
Source: The authors.

3.1.2   Pipeline for Single Particle Configuration

During the course of this work, the fluidic solutions introduced inside the acoustic chamber generally contained around 100 particles. A particle-to-particle interaction caused the appearence of grouped packs of particles, which makes it difficult to carry out the experiments. To achieve a single-particle configuration, a sequence of two steps was carefully followed. Firstly, once a pack of particles started to emerge, the actuator power was turned off. Lastly, about 10 seconds later, the device was turned on again, causing only a single particle to be trapped at the acoustic wave pressure node. Through this pipeline the proposed experiments could be successfully conducted.

3.2   Calibration

As it was already discussed, the density of a particle can be measured by a model based on the fall process inside a microfluidic cavity along with a confocal optical inspection. As the particle falls, the relative distance to the image confocal plane becomes larger. This results in a blurring effect, which increases the particle size in the image as it gets increasingly defocused.

To analyze the dynamics of a particle with a specific diameter and unknown density, it is necessary to use a calibration curve that relates the relative area of a particle, which

Figure 3.2: Illustration of how the calibration procedure works.
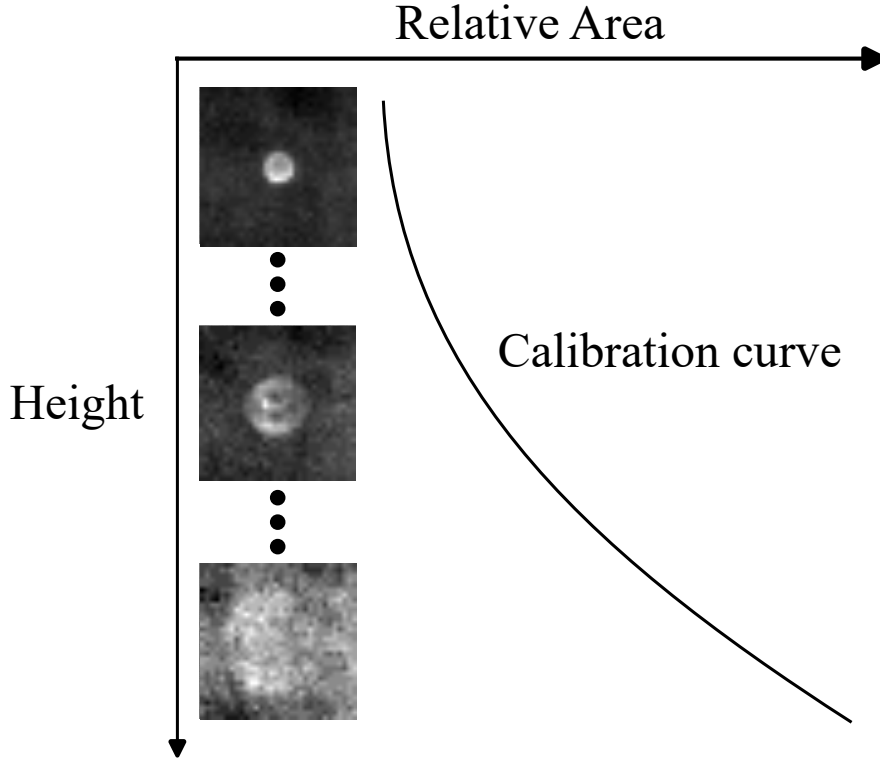
Source: The authors.

has the same diameter, with previously known heights between particle and the resonant cavity bottom during a fall process, as exposed in Figure 3.2. Considering that we have n (18 were used in the calibration step of the experiment) acquired images from a particle during fall and its respective heights and areas, relative area values can be computed by the following equation:

$$A_{relative} = \frac{A_i - A_1}{A_n - A_1} \tag{3.1}$$

where A_1, A_i and A_n are, respectively, area values for the first, current and last captured images.

Therefore, the computed values for relative area and height can be fitted to a double exponential function, which is defined as follows:

$$h = \alpha_1 \exp\left[-\frac{A_{relative}}{\beta_1}\right] + \alpha_2 \exp\left[-\frac{A_{relative}}{\beta_2}\right] + \omega_0 \tag{3.2}$$

where α_1, α_2, β_1, β_2 and ω_0 can assume arbitrary values, having no physical meaning. The resulting curve can be later used to estimate height values for a new particle by applying as input the relative area values during a fall experiment. Lastly, we can derive the obtained height values to estimate the falling velocity for that particle and with Eq. (2.6), find its density.

3.3   Data Preprocessing

As the acquired microscope images are very noisy and defocused and also has a low contrast level, they are generally not in ideal conditions for use in experiments. Therefore, before the curve fitting and optimization steps we applied some preprocessing steps in order to have a better set of input images:

- Particle Alignment: The particles were aligned at the center of the respective image. This reduces the number of hyperparameters that need to be optimized, as μ_x and μ_y will be fixed to zero.

- Image Resizing: The images were resized to a 32×32 shape, leading to a reduction in the search space for the optimization step.

- Contrast Enhancement: This step was done through the subtraction of a mean background value of the image.

3.4   Curve Fitting

An important aspect of the particle area measurement process is that it is done manually, being more susceptible to errors. This problem could be overcome through the usage of a procedure to automatically compute the particle area in the captured image. Aiming to achieve such solution, during this step of the work the feasibility of fitting curves to the particle area in an input image was investigated. The tests focused mainly in the application of 2D Gaussian functions for this task, which were previously discussed and defined by Eq. 2.8.

The idea is to fit the Gaussian model into the image by minimizing the Mean Squared Error (Eq. 2.12) between the Gaussian and each pixel in the image. This technique is very powerful provided that the noise is symmetric. Regardless of the amplitude of the noise present in the image the model will have minimum MSE only when the parameters of the Gaussian fit as best as possible with the object in the image.

Once fitted, the Gaussian parameters can be used to give us measures on the object like its position (mean of the Gaussian) and size (standard deviation).

3.5   Optimization

As stated before, defining a Gaussian function that suits the particle in an input image is not trivial. Hence, we delegated the task of finding parameters that best fit a specific particle image to optimization algorithms. As the particle was already centered in the image, we only optimized the amplitude (p) and the variance (σ^2) of the Gaussians for

each image. The experiment set was comprised of 13 consecutive images acquired from a fall process of a polysterene bead with same diameter as the one used in calibration.

Firstly, a Genetic Algorithm was applied using the following configuration:

- Generations: executed for 1000 generations;

- Population: 100 individuals (vectors $[p, \sigma^2]$);

- Mutation Rate: a mutation rate of 1% was applied.

The fitness of each individual was measured by the Mean Squared Error between the processed image and the Gaussian curve created with the current parameter values.

As the genetic algorithm is not deterministic, it may not reach the global minimum of the error function. Thus, a natural step is to apply a more controlled optimization method having as a starting point the best parameters found for each image by the GA. For this task we tested the application of a Stocastic Gradient Descent Bottou (2012) optimizer for p and σ^2 parameters. For the Gradient Descent the following configuration was used:

- Epochs: the process was executed for 1000 epochs;

- Learning Rate: Taking into account that the genetic algorithm achieved results close to a global minimum, the curve gradient at this point will have very small values. To tackle this scenario, we used a higher learning rate value of 2.0;

- Loss Function: Mean Squared Error (MSE).

This process was executed for each set of test images and initial parameters.

Chapter 4

Results and Discussions

Figure 4.1: Curve obtained by fitting an exponential function to height and relative area values during the calibration process.
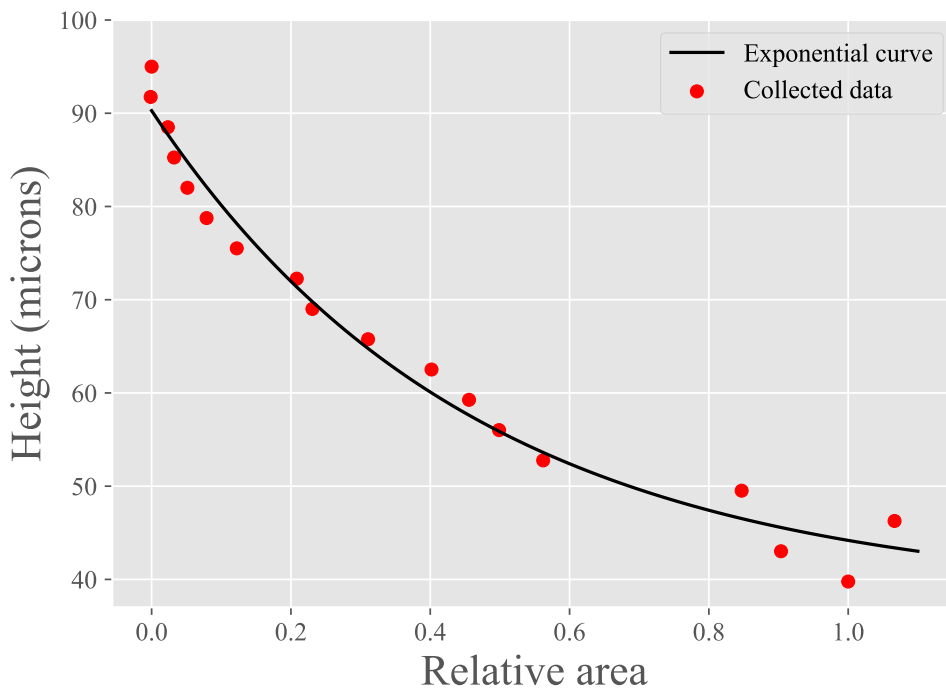
Source: The authors.

By applying the proposed methodology, we were able to obtain a calibration curve for the experiment. With the usage of ground-truth images, where particle's contour was previously known, we extracted particle's radius from a pixel-micron relation. Then, we calculated area values by considering the particle as a perfect circle and, along with it's respective height values, we could generate a calibration curve that related particle height with relative area, as discussed in section 3.2. Numerically fitting the points to the proposed double exponential function (Eq. (3.2)), we could achieve the curve shown in Fig. 4.1.

Figure 4.2: Image grid showing the results for diameter estimation. First row: Original images (last 8 slices from left to right – ie. heights). Second row: Processed images. Third row: Contours obtained with the Genetic Algorithm. Bottom row: Contours found using the Gradient Descent approach.
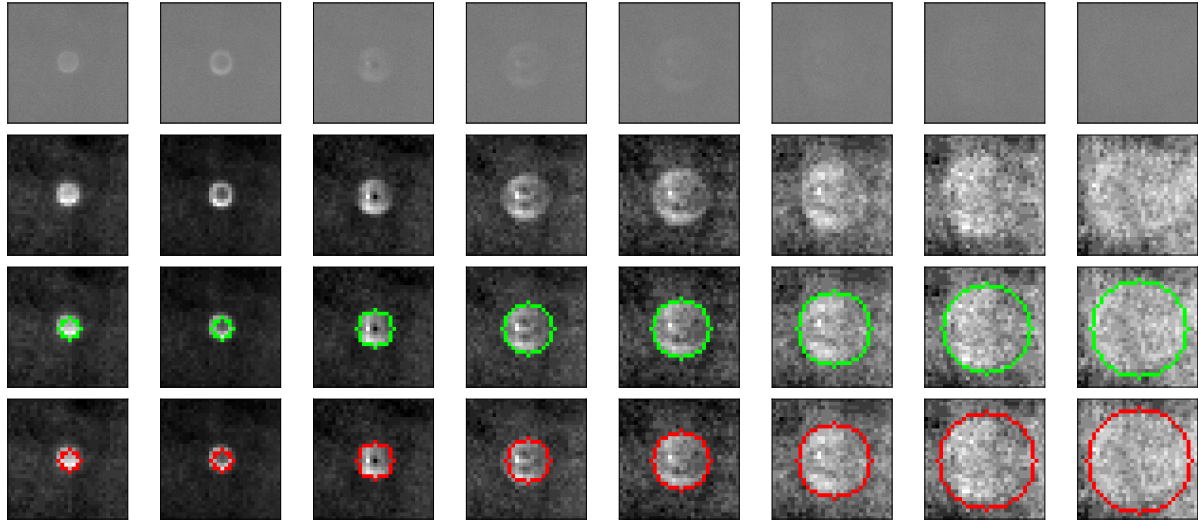
Source: The authors.

After the application of the pipeline proposed in Section 3.5, we could achieve good results for all test images. Figure 4.2 presents an image grid containing results for eight of the thirteen tested images. Despite being stochastic, the genetic algorithm was able to find good parameters for the 2D Gaussian functions. As shown in the second row of Fig. 4.2, the contours of resulting Gaussian curves seem to fit, if not perfectly match, the particle contour. The results are even more interesting for the last images of the sequence, where we find a high amount of noise and a clear contour for the particle is not visually identifiable. Still, the algorithm was able to find plausible parameters for the Gaussian.

The application of the Stochastic Gradient Descent optimizer did not change the results in general. Despite giving a lower loss value, the resulting Gaussian curve was practically the same. The only exceptions were the results for three of the thirteen

Figure 4.3: Noisy image (left). The genetic algorithm result is highlighted in green (middle) while the gradient optimization is in red (right). Although it is not trivial to spot the particle visually, the genetic algorithm was able to identify a plausible contour.
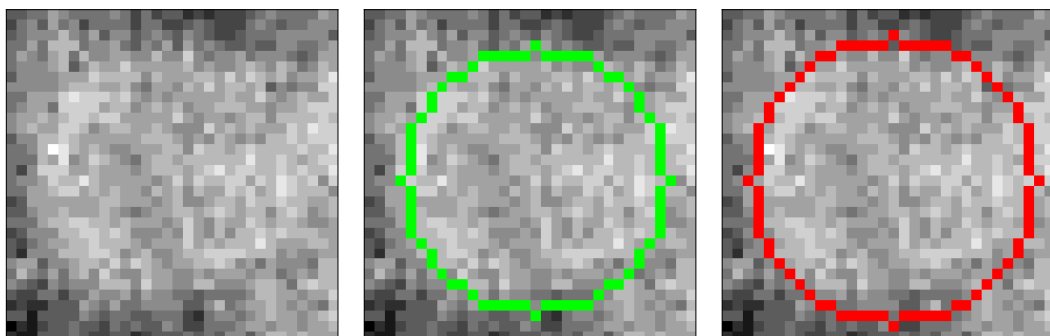
Source: The authors.

test images, which are shown in fourth, seventh and eighth columns of Fig. 4.2. The optimization produced a visible result, since curve contours changed slightly with respect to the ones found by the genetic algorithm. However, for all other images, the plotted Gaussian contour was exactly the same, which ratifies the good result found by the genetic approach. In Fig. 4.5 we can see resulting loss curves for the parameter tuning process.

Figure 4.4: Estimated height for each image by applying computed Gaussian areas as input to the calibration curve.
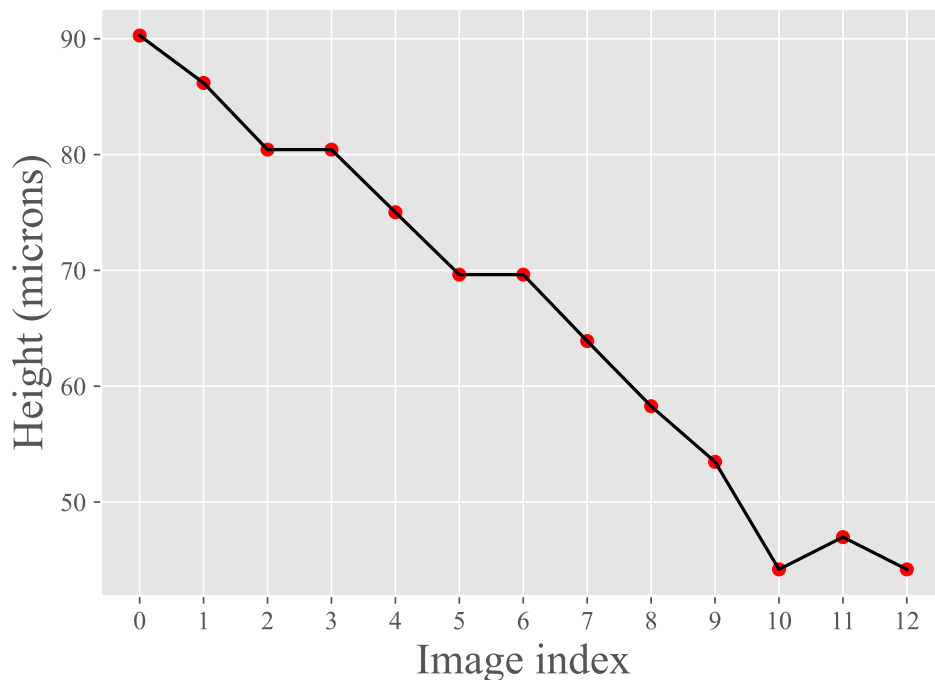
Source: The authors.

Lastly, we used the obtained Gaussian curves to compute particles' areas in each image and generate relative area values by applying Eq. (3.1). Such values could then be used as input for the calibration curve discussed in Section 3.2 to estimate particle's height at each image, which are shown in Figure 4.4.

Then, we numerically derived the height curve and applied the mean value as particle's velocity in Eq. (2.6) to compute the particle's density. For this computation we also used a gravitational acceleration of $g = 9.82$ m·s^{-2} along with previously discussed values of $\rho_{fluid} = 997$ kg·m^{-3} and $\mu = 0.89 \times 10^{-1}$ Pa·s. This procedure resulted in a density value of 1059 kg·m^{-3}, which is close to the real density value of 1050 kg·m^{-3}, corresponding to an error of 0.8%.

Such result ratifies our approach as a valid mean to estimate the area of a particle and its density by applying the previously described equations. It is worth mentioning that even in extreme cases, where the particle was not easily identifiable and the image contained a lot of noise, the proposed method was capable of giving good estimates for

Gaussian curve approximation for the particle, consequently allowing the computation of it's density.

Figure 4.5: Example of loss curves during the parameter optimization process. Plots show, respectively, results for genetic algorithm and gradient descent steps.
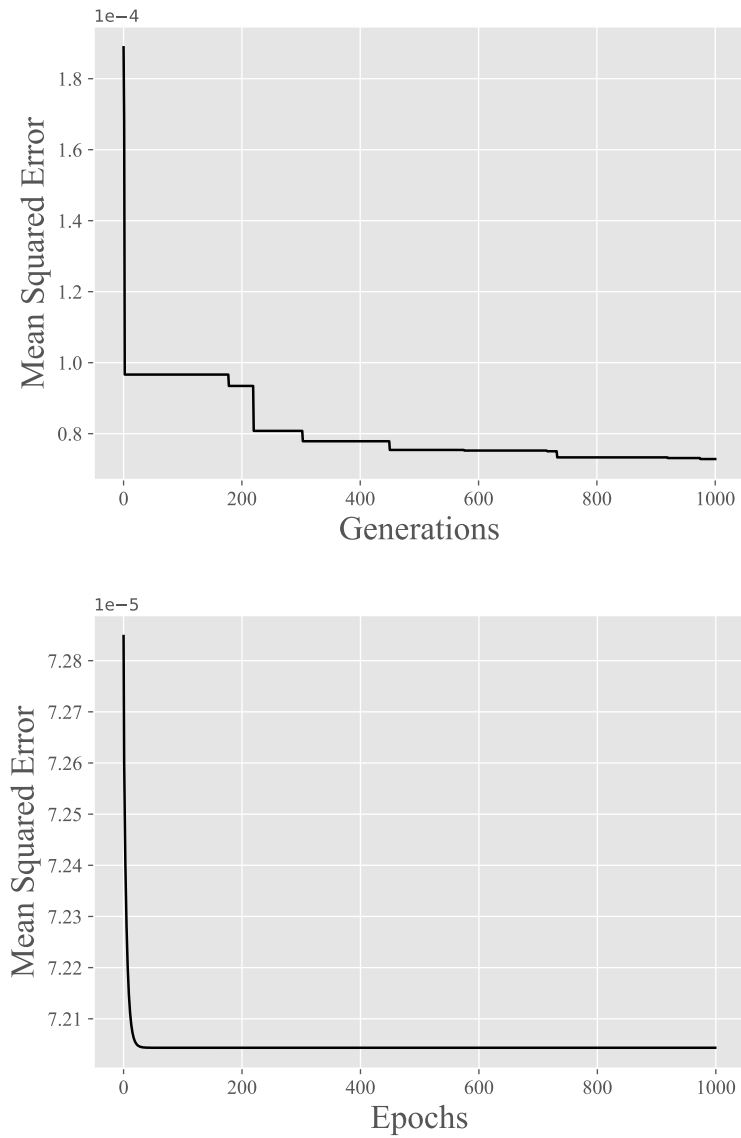
Source: The authors.

Conclusion

The discussed work presented a methodology to obtain a sub-micron particle's density using acoustofluidics. This approach is traditionally performed manually, which renders the development of point-of-care devices unfeasible.

Aiming at automating the process, the usage of 2D Gaussian fitting was proposed to retrieve particle's diameters throughout different positions during fall as an alternative to analyze its velocity and compute its density. After a calibration procedure, the fall dynamics was analyzed and the diameters were used as inputs to the calibration function in order to obtain the corresponding depths along time. This fall velocity is used alongside different parameters in a given formulation to compute the density. Given a reference known value of 1050 kg·m^{-3} the method provided a value of 1059 kg·m^{-3}, satisfactorily close to the calibration density. As future work, we intend to analyze the usage of blur score metrics related to Gradient, Laplacian, Fourier Transform and wavelets as an approach to the discussed particle fitting problem.

Bibliography

Ananthanarasimhan, J., Raghuram, A., and Rao, L. (2022). Arc diameter estimation of a rotating gliding arc using a simple high–speed camera and "gaussian fit" function. *IEEE Transactions on Plasma Science*, 50(6):1401–1406.

Anniballe, R. and Bonafoni, S. (2015). A stable gaussian fitting procedure for the parameterization of remote sensed thermal images. *Algorithms*, 8(2):82–91.

Bose, N., Zhang, X., Maiti, T. K., and Chakraborty, S. (2015). The role of acoustofluidics in targeted drug delivery. *Biomicrofluidics*, 9:052609.

Bottou, L. (2012). Stochastic gradient descent tricks. In *Neural networks: Tricks of the trade*, pages 421–436. Springer.

Bryan, A. K., Goranov, A., Amon, A., and Manalis, S. R. (2010). Measurement of mass, density, and volume during the cell cycle of yeast. *Proceedings of the National Academy of Sciences*, 107(3):999–1004.

Bui, T. M., Coron, A., Mamou, J., Saegusa-Beecroft, E., Machi, J., Dizeux, A., Bridal, S. L., and Feleppa, E. J. (2015). Level-set segmentation of 2d and 3d ultrasound data using local gamma distribution fitting energy. In *2015 IEEE 12th International Symposium on Biomedical Imaging (ISBI)*, pages 1110–1113.

Byttner, W. (2019). Classifying rgb images with multi-colour persistent homology.

Dai, T., Ma, T., Liu, H., Cui, J., Liu, Y., Wei, Q., Wu, J., Wang, S., and Jin, Y. (2010). Low-cost high-resolution animal spect imaging on a clinical spect scanner. In *2010 3rd International Conference on Biomedical Engineering and Informatics*, volume 1, pages 341–344.

Fan, Y., Wang, X., Ren, J., Lin, F., and Wu, J. (2022). Recent advances in acoustofluidic separation technology in biology. *Microsystems & Nanoengineering*, 8:94.

Kizel, F., Shoshany, M., and Netanyahu, N. S. (2015). Spatially adaptive hyperspectral unmixing based on sums of 2d gaussians for modelling endmember fraction surfaces. In *2015 IEEE International Geoscience and Remote Sensing Symposium (IGARSS)*, pages 4440–4443.

Konak, A., Coit, D. W., and Smith, A. E. (2006). Multi-objective optimization using genetic algorithms: A tutorial. *Reliability engineering & system safety*, 91(9):992–1007.

Lei, Z., Chen, X., and Lei, T. (2016). Sub-pixel location of motion blurred weak celestial objects in optical sensor image based on elliptical 2d gaussian surface fitting. In *2016 International Conference on Industrial Informatics - Computing Technology, Intelligent Technology, Industrial Information Integration (ICIICII)*, pages 100–104.

Li, P., Mao, Z., Peng, Z., Zhou, L., Chen, Y., Huang, P.-H., Truica, C. I., Drabick, J. J., El-Deiry, W. S., Dao, M., Suresh, S., and Huang, T. J. (2015). Acoustic separation of circulating tumor cells. *Proceedings of the National Academy of Sciences*, 112:4970–4975.

Santos, H. D. A., Silva, G. C., Vieira, T. F., Silva, A. E., de Araújo, B. Q., Jacinto, C., Rocha, U., Alexandre-Moreira, M. S., and Silva, G. T. (2021). Measuring cell density in a acoustofluidic microcavity. In *2021 IEEE UFFC Latin America Ultrasonics Symposium (LAUS)*, pages 1–4.

Wang, Z., Wang, H., Becker, R., Rufo, J., Yang, S., Mace, B. E., Wu, M., Zou, J., Laskowitz, D. T., and Huang, T. J. (2021). Acoustofluidic separation enables early diagnosis of traumatic brain injury based on circulating exosomes. *Microsystems & Nanoengineering*, 7:20.

Zhao, Y., Lai, H. S. S., Zhang, G., Lee, G.-B., and Li, W. J. (2014). Rapid determination of cell mass and density using digitally controlled electric field in a microfluidic chip. *Lab Chip*, 14:4426–4434.